The Phosphoproteome of the Degenerating rd1 Retina Changes After Protein Kinase G Inhibition

Jiaming Zhou , Charlotte Welinder , Per Ekström *

Posted Date: 12 May 2023

doi: 10.20944/preprints202305.0896.v1

Keywords: retinitis pigmentosa; cell death,; phosphoproteomic

Article

The Phosphoproteome of the Degenerating *rd1* Retina Changes after Protein Kinase G Inhibition

Jiaming Zhou [1,*], Charlotte Welinder [2] and Per Ekström [1]

[1] Ophthalmology, Department of Clinical Sciences, Lund, Lund University, Sweden
[2] Faculty of Medicine, Department of Clinical Sciences Lund, Mass Spectrometry, Lund University, Lund, Sweden
* Correspondence: jiaming.zhou@med.lu.se

Abstract: Retinitis pigmentosa (RP) is a frequent cause of blindness among the working population in industrial countries, due to the inheritable death of photoreceptors. Though a gene therapy was recently approved for mutations in the RPE65 gene, there is generally no effective treatment presently. Previously, abnormally high-level cGMP and overactivation of its dependent protein kinase (PKG) have been suggested as causative for the fatal effects on photoreceptors, making it meaningful to explore the cGMP-PKG downstream signaling for more pathological insights and novel therapeutic target development purposes. Here we manipulated the cGMP-PKG system in degenerating retinas from the *rd1* mouse model pharmacologically via adding a PKG inhibitory cGMP-analogue to organotypic retinal explant cultures. A combination of phosphorylated peptides enrichment and mass spectrometry was then applied to study the cGMP-PKG-dependent phosphoproteomics. We identified a host of novel potential cGMP-PKG downstream substrates and related kinases using this approach, and selected the RAF1 protein, which may act as both a substrate and a kinase, for further validation. We showed that the RAS/RAF1/MAPK/ERK pathway may be involved in retinal degeneration in a yet unclarified mechanism, thus deserving further investigation in the future.

Keywords: retinitis pigmentosa; cell death; phosphoproteomic

1. Introduction

The hereditary disease Retinitis pigmentosa (RP) is a frequent cause of blindness among the working population in industrial countries [1]. There is no effective treatment available at present [2], with the notable exception of the approved gene therapy for mutations in the RPE65 gene [3]. RP results in vision loss via fatalities of the light-sensing photoreceptors, which are categorized as rods and cones. The degeneration pattern starts with the death of rods that cause night blindness, which is followed by the degeneration of cones [4] and hence loss of general vision. The *rd1* mouse model, with the gene mutation of the beta subunit of the enzyme phosphodiesterase-6 (PDE6), is characterized by an abnormally high level of photoreceptor cyclic guanosine monophosphate (cGMP) and a rapid loss of these cells [5]. The degeneration of photoreceptors in this phenotype has been demonstrated with an increasing decline in outer retinal thickness, and overall amplitude reduction in the waveform via spectral domain optical coherence tomography [6] and electrophysiological changes [7], respectively. Although the details on how the high level of cGMP affects the photoreceptors are still not known, previous studies have suggested that at least part of the death-promoting impact on photoreceptors could be exerted via increased activity of cGMP-dependent protein kinase (PKG), probably causing over-phosphorylation within photoreceptors [8,9]. It would thus be most helpful if this could be studied more closely.

There are two forms of PKG, PKG1 and PKG2, with PKG1 having two isoforms, PKG1alpha and PKG1beta [10]. cGMP-PKG functions by phosphorylation of certain serine and threonine residues in a number of biological targets [10]. The importance of this so-called cGMP-PKG system has been

 doi:10.20944/preprints202305.0896.v1

recognized for its essential role in gene regulation in diverse tissues [11,12], and also for its involvement in the cell death mechanism [13]. Despite the deepening insights regarding this system, we are as indicated above still confronted with one unsolved problem, namely, what are the actual details of the downstream signaling of the cGMP-PKG system that could affect the RP progression?

Certain analogues of cGMP, a category of chemically modified versions of the native cGMP [14–16], exert considerable inhibition or activation of PKG isoforms. This has been taken advantage of when testing potential treatments, where the systemic administration of a selected liposome-formulated cGMP analogue with PKG inhibitory properties was shown to protect RP retinas from retinal degeneration and to preserve the photoreceptor function [9]. To reveal the downstream signaling practically, one may thus manipulate the retinal cGMP-PKG system pharmacologically via the addition of relevant cGMP-analogues during organotypic retinal explant culturing, and subsequently, explore the cGMP-PKG downstream pathways with a phosphoproteomic analysis, in analogy with how the effects of PKG manipulation on the retinal transcriptome has been studied [17]. Together this should be beneficial for studying the cGMP-PKG-dependent targets.

In this study, we have therefore used a PKG inhibitor on *rd1* retinal explants, and via a phosphoproteomic analysis, which combined phosphopeptide enrichment with mass spectrometry (MS) [18], compared the resulting phosphopeptide pattern with that of the untreated counterparts. The selected lists of altered phosphorylated sites after PKG inhibition were then further analysed via appropriate bioinformatics methods to reveal the downstream pathways that were potentially connected to RP advancement. To study the possible effectors of cGMP-PKG system in RP, we subsequently picked up several phosphorylated proteins for further validation of phosphorylation. Our results show a number of phosphorylated sites that are potentially controlled by cGMP-PKG in the *rd1* retina, and as such provide more insights into the retinal degeneration mechanisms in RP.

2. Materials and methods

2.1. Animals

The C3H/*rd1*/*rd1* (*rd1*; [19]) and control C3H wild-type (wt; [19]) were kept and bred in house under standard white cyclic lighting, with free access to food and water, and used irrespective of sex. Day of birth of the animal was considered as postnatal 0 (P0), with the day following this considered as P1, *etc*.

2.2. Organotypic retinal explant culture

Mice were exposed to carbon dioxide (CO_2) to minimize the suffering before Euthanasia. Retinas from P5 mice were used to generate explants according to our standard protocol [17]. Inserts with the explants were put into six-well culture plates with 1.5 mL serum-free medium in each well. Plates were incubated at 37° C with a 5% CO_2 atmosphere, and the medium was replaced every two days. No additions were made to the cultures for the first 2 days. One group of the cultures, which at this point were at an age corresponding to P7, where then exposed to 50 µM Rp-8-Br-PET-cGMPS (PKG inhibitor; Biolog, Bremen, Germany, Cat. No.: P 007) for the following 4 days, with the end point thus equivalent to P11 (n=4), with their corresponding controls (n = 4) receiving the same amount of distilled water. Another group (n = 4) was exposed to the Rp-8-Br-PET-cGMPS with the same concentration but only for 2 hours before the end of the protocol, with controls (n = 4) similarly exposed to distilled water. All retinal explants were either collected for protein extraction followed by phosphoproteomic analyses. In parallel, another 4 groups of *rd1* explants, reaching a total of 13 explants, were generated, with 4 such in the group of retinas with 4 days of PKG inhibition and 3 each in the other 3 groups. These explants were fixed, sectioned, and used for microscopy-based studies.

Animals were randomly assigned to the experimental groups, and the experimenters were aware of the conditions of the animals during retinal explant culture. No statistical method was applied to predetermine the sample size of the experimental groups. The sample size was chosen

 doi:10.20944/preprints202305.0896.v1

based on relevant literature in the field as well as on ethical considerations. The study was not pre-registered. The study was exploratory without exclusion criteria being pre-determined.

2.3. Sample preparation for MS

A total of 16 retinal explants were used for MS measurement, and 4 explants were used per group. The experimenter was unaware of the explant's group during experimentation. Each explant was homogenized separately in buffer (50 mM Tris-HCl, 50 mM NaCl, 1 mM EDTA, 5 mM NaH_2PO_4, 1 mM DL-Dithiothreitol (DTT)), supplemented with phosphatase inhibitors (Lot No, 33041800, Roche, Basel, Switzerland, 1 tablet per 10 mL buffer) using a homogenizer (Knotes Glass Company, Vineland, NJ). The homogenate was then centrifuged at 10 000 g for 5 min at 4°C. The soluble fraction was collected after centrifugation, with the concentration measured by Bio-Rad Protein Reagent Assay Kit (Cat. No.: #5000113, #5000114, #5000115, Bio-Rad, Hercules, CA).

For each separated sample, proteins were reduced with DTT to a final concentration of 10 mM and heated at 56 °C for 30 min followed by alkylation with iodoacetamide for 30 min at room temperature in the dark to a final concentration of 20 mM. Subsequently, samples were precipitated with ice cold ethanol for overnight at -20°C followed by centrifugation at 14 000 x g for 10 min. The pellets were resuspended in 100 mM ammonium bicarbonate and sonicated for 20 cycles of 15 sec on, 15 sec off, using a Bioruptor (Diagenode, Denville, NJ). Digestion was performed by adding trypsin (Sequencing Grade Modified Trypsin, Part No. V511A, Promega, Madison, WI) in a ratio of 1:50 to the samples and incubated for overnight at 37 °C. The digestion was stopped by the addition of 5 µL 10% trifluoroacetic acid (TFA).

The Pierce High-Select Fe-NTA Phosphopeptide Enrichment Kit (Cat. No.: A32992; Thermo Fischer Scientific, Waltham, MA) was used to enrich phosphopeptides according to the manufacturer's protocol. The phosphopeptides were run in a Speed Vac to dryness and resolved in 2% acetonitrile (ACN) and 0.1% TFA to a peptide concentration of 0.25 µg/µL.

2.4. MS acquisition and analysis

The peptide analyses were performed on a Q Exactive HFX mass spectrometer (Thermo Scientific) connected to an EASY-nLC 1200 ultra-high-performance liquid chromatography system (Thermo Scientific). Peptides, 1 µg, were separated on an EASY-Spray column (Thermo Scientific; ID 75µm × 50 cm, column temperature 45°C) operated at a constant pressure of 800 bar. A two-step gradient of buffer B (80% acetonitrile, 0.1% formic acid) in buffer A (aqueous 0.1% formic acid) was applied at a flow rate of 300 nl min-1. In the first step a gradient of 10 to 30% of buffer B was run for 90 min followed by a 30 to 45% gradient of buffer B in 20 min. One full MS scan (resolution 60,000 @ 200 m/z; mass range 350–1,400m/z) was followed by MS/MS scans (resolution 15,000 @ 200 m/z). The precursor ions were isolated with 1.3 m/z isolation width and fragmented using higher-energy collisional-induced dissociation at a normalized collision energy of 28. Charge state screening was enabled, and singly charged ions as well as precursors with a charge state above 6 were rejected. The dynamic exclusion window was set to 10 s. The automatic gain control was set to $3e^6$ for MS and $1e^5$ for MS/MS with ion accumulation times of 45 ms and 60 ms, respectively. The intensity threshold for precursor ion selection was set to $1.7e^4$.

The raw DDA data were analyzed with Proteome Discoverer™ Software (Version 2.3, Thermo Fisher Scientific). Peptides were identified using both SEQUEST HT and Mascot against UniProtKB mouse database (UP000000589 plus isoforms). The search was performed with the following parameters applied: static modification: cysteine carbamidomethylation and dynamic modifications: N-terminal acetylation. Phosphorylation (S, T, Y, for serine, threonine and tyrosine, respectively) was set as variable for the phosphopeptide analysis. Precursor tolerance was set to 10 ppm and fragment tolerance to 0.02 ppm. Up to 2 missed cleavages were allowed and Percolator was used for peptide validation at a q-value of maximum 0.05. Peptides with different amino acid sequences or modifications were considered as unique. Extracted peptides, with a quality q-value lower than 0.05, and modification of S, T, and Y phosphorylation detected were used to identify and quantify them

 doi:10.20944/preprints202305.0896.v1

by label-free relative quantification. The extracted chromatographic intensities were used to compare peptide abundance across samples.

The MS results were processed via Perseus software (version 1.6.0.7, Tyanova et al., 2016). The protein intensities were log2 transformed. Selective criteria were defined as: Among 4 replicates of 4 conditions (16 samples totally), only a peptide with the missing value of less than 30% in total (less than 5 samples with missing value) would be selected and the missing values were replaced from a normal distribution was performed though data imputation by using the following settings: width 0.3 and downshift 0. The further bioinformatics analysis of these processed data was done via the web-based tool Phosphomatics (https://phosphomatics.com/; [20]). In Phosphomatics, two-Sample Student's t-test (two-tailed) were performed to compare phosphorylated site levels between the *rd1* explants with 2 hours of PKG inhibition vs untreated control, and 4 days of PKG inhibition vs untreated controls. A p-value of 0.05 was defined as the cut-off. Two lists of the phosphorylated sites identified previously were used to perform a further upstream kinase analysis in Phosphomatics. The biological pathways that might be affected between *rd1* untreated and *rd1* with PKG inhibition samples were determined in Enrichr (https://maayanlab.cloud/Enrichr/), where differentially phosphorylated sites mentioned above were used as input list to perform pathway-based analysis of Kyoto Encyclopedia of Genes and Genomes (KEGG).

2.5. Cryosection, immunohistochemistry and Proximity ligation assay (PLA)

Retinal tissues from *rd1* and wt *in vivo* at P9, as well as P11 cultured explants from *rd1*, were treated with 4% formaldehyde for 2 hours, washed 3 × 15 min in phosphate-buffered saline (PBS), cryoprotected in PBS + 10% sucrose for overnight at 4 °C and subsequently with PBS + 25% sucrose for 2 hours. After embedding in a medium with 30% bovine serum albumin (BSA; Cat. No.: A5253-250G; Sigma-Aldrich, St. Louis, MO, USA) and 3% gelatine (Cat. No.: 1040781000, Merck Millipore, Burlington, MA, USA) mixed in H_2O, 12 µm thick retinal cross-sections were cut and collected from a HM560 cryotome (Microm, Walldorf, Germany). The sections were stored at -20 °C for later usage. Cryosections were then used for immunostaining and PLA. Totally 10 retinal samples were used, with 5 each in either *rd1* or wt strains, while 13 *rd1* explants were used, with 4 in group of retinas with 4 days of PKG inhibition and 3 each in other 3 groups.

For immunostaining, briefly, the cryosections were dried in room temperature for 15 minutes and rehydrated in PBS. Then they were blocked with 1% BSA + 0.25% Triton X100 + 5% goat serum in PBS at room temperature for 45 min. The primary antibody anti-Raf1 (Cat#: MA5-17162, ThermoFisher) was diluted with 1% BSA and 0.25% Triton X100 in PBS (PTX) and incubated at 4 °C for overnight; a no primary antibody control ran in parallel. Sections were washed 3 × 5 min each in PTX and incubated with a donkey anti-mouse IgG (H+L) highly cross-adsorbed secondary antibody, Alexa Fluor™ Plus 488 (#A32766, ThermoFisher) at 1:800 dilution in PTX. After 3 x 5-min PBS washes the sections were mounted with Vectashield DAPI (Vector, Burlingame, CA, USA).

The PLA, which detects if two antigens are in close proximity (<40 nm) with each other, was performed on cryosections, using Detection Reagents Red kit (DUO92008-100RXN, Merck, Readington Township, NJ), the PLA Probe anti-rabbit PLUS (DUO92002, Merck, Readington Township, NJ) and anti-mouse MINUS (DUO92004, Merck, Readington Township, NJ). The procedure followed the manufacturer's instructions. In short, the retinal sections were blocked with blocking solution (provided in PLA Probe kit) for 45 min at 20°C, and primary antibodies antibody anti-Raf1 (Cat#: MA5-17162, ThermoFisher) and anti-Phosphoserine (ab9332, Abcam, Cambridge, UK) were incubated overnight at 4°C. PLA Probe anti-rabbit PLUS and anti-mouse MINUS were incubated for 1 hr at 37°C. The ligation and amplification steps were performed using the Detection Reagents Red, followed by the addition mounting of Vectashield DAPI (Vector, Burlingame, CA, USA).

2.6. Microscopy and image processing

A Zeiss Imager Z1 Apotome Microscope (Zeiss, Oberkichen, Germany), with a Zeiss Axiocam digital camera was used for microscopy observations. Image generation and contrast enhancement

 doi:10.20944/preprints202305.0896.v1

were performed identically for all images via the ZEN2 software (blue edition). The immunostaining was analysed for staining differences via three sections each from three to five animals for each condition, after which the fluorescent intensities of positive cells randomly distributed within in the area of interest (outer nuclear layer, ONL, *i.e.* the photoreceptor layer) were assessed. Fluorescence intensity was captured and analysed by the ImageJ software (version 1.53a, NIH, Maryland, USA). The freehand selection function was used to target the ONL, after which the fluorescence intensity was calculated with the measure function. The values of all sections from the same animal were averaged. For PLA, the images were also generated with the aid of a Zeiss Imager Z1 Apotome Microscope and the ZEN2 software (blue edition). The punctuations of ONL, which represent reaction products from when the two antigens are in close proximity, was counted manually of three sections each from three to five animals for each condition, with values from the same animal averaged. The experimenter was unaware of the groups of the samples during image processing.

2.7. Statistical analysis

The student's t-test was used to compare the values of immunostaining intensities and PLA punctuations in different conditions in R, and p value cutoff was defined as 0.05. Visualization of KEGG analysis was also performed in R.

3. Results

3.1. Quantitative phosphoproteomics of retinal explants with PKG inhibition

In total 17915 phosphorylated sites and 3405 retinal proteins were identified (Figure 1A), among these, 10352 phospho sites from 2214 proteins were selected for further analysis, according to the defined criteria (detailed in Materials and Methods). Comparison via Student's t-test showed that 299 phospho sites of 108 proteins had decreased phosphorylation, while 184 phospho sites of 83 proteins had increased phosphorylation, in retinas with PKG inhibition for 2 hours compared to their untreated counterparts (Figure 1B, Table 1; see Supplementary Table S1 for full list, with phosphorylation sites, fold changes etc.). For the longer treatment, 4 days, 98 phospho sites of 46 proteins were observed with decreased phosphorylation, while 265 phosphorylation sites of 130 proteins with increase phosphorylation. corresponding numbers were 98 and 265 phospho sites, in 46 and 130 proteins, respectively (Figure 1C, Table 2 and Supplementary Table S2 for full list).

There were 5 overlapping proteins with decreased phosphorylation after both 2 hours (short term) or 4 days (long term) PKG inhibition. (Figure 1D and Table 1; overlapping proteins highlighted in yellow in Supplementary Tables S1 and S2). For proteins with increased phosphorylation, there were 16 overlapping proteins after short and long term PKG inhibition (Figure 1E and Table 2; overlapping proteins highlighted in yellow in Supplementary Tables S1 and S2). When we focused on individual phosphorylation sites in the peptides of the overlapping proteins, there were 2 proteins with decreased phosphorylation that were represented by the very same, specific phosphorylation sites at both timepoints, and 3 proteins from those with increased phosphorylations (Tables 1 and 2; plus labelled with green in Supplementary Tables S1 and S2).

Preprints (www.preprints.org) | NOT PEER-REVIEWED | Posted: 12 May 2023 doi:10.20944/preprints202305.0896.v1

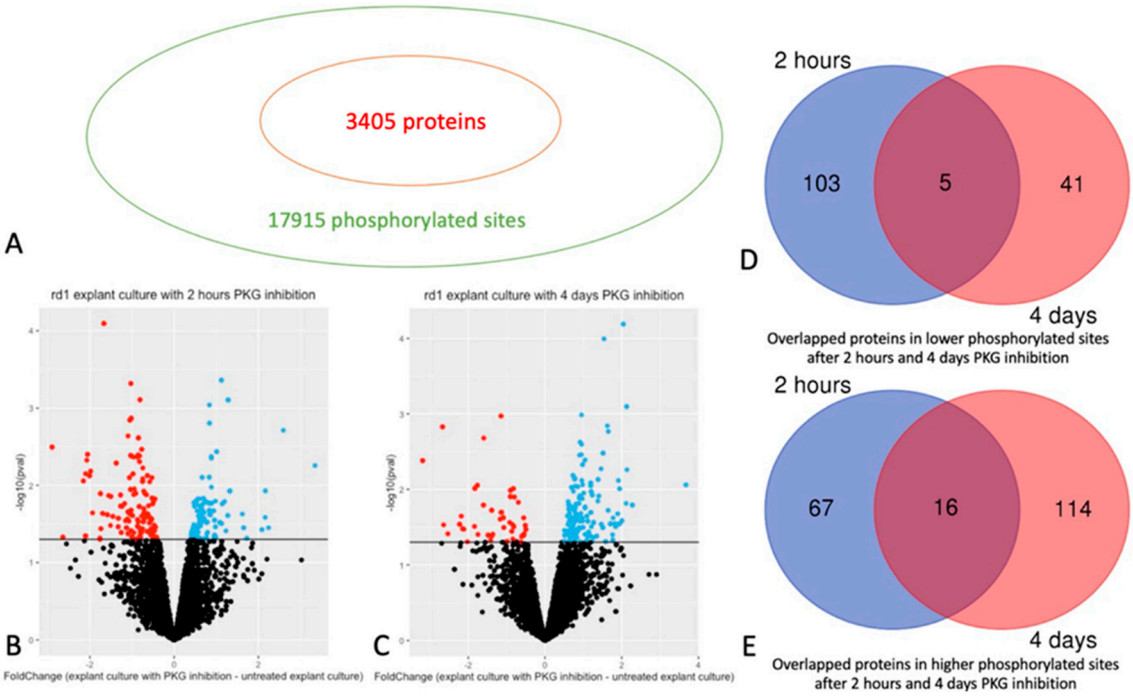

Figure 1. Phosphorylated sites and proteins in retinal explants affected by PKG inhibition. Retinal explants generated from the rd1 strain were treated with PKG inhibitor for 2 hours or 4 days, and phosphoproteomics was done via mass spectrometry (MS) after phosphopeptide enrichment. A: 17915 phosphorylated sites of 3405 proteins were identified. B: Volcano plot showing Fold Change between and -Log10(p-value) of phosphorylated sites with 2 hours treatment. C: Volcano plot showing Fold Change between and -Log10(p-value) of phosphorylated sites with 4 days treatment. For both B and C red and blue dots represent sites with decreased or increased phosphorylation, respectively ($p < 0.05$), while black dots represent sites without difference. D: Venn diagram showing the overlapped proteins in decreased phosphorylated sites after 2 hours and 4 days PKG inhibition. E: Venn diagram showing the overlapped proteins in increased phosphorylated sites after 2 hours and 4 days PKG inhibition.

Table 1. Lists of proteins showing decreased phosphorylation after PKG inhibition for either 2 hours (left column) or 4 hours (center column), whereas the right column shows proteins that showed reduced phosphorylation at both time points. Note that the left and center columns only show the 20 proteins with highest fold change for 2 hours and 4 days, respectively. The total number of proteins with decreased phosphorylation was 108 and 46 after 2 hours and 4 days PKG inhibition, respectively. Full lists of all proteins/peptides with decreased phosphorylation are found in Supplementary Tables S1 and S2.

Proteins with decreased phosphorylation after PKG inhibition									
Top 20 after 2 hours				**Top 20 after 4 days**				**Appearing in both**	
Gene symbol	**Protein name**	**Fold Change**	**p-value**	**Gene symbol**	**Protein name**	**Fold Change**	**p-value**	**Gene symbol**	**Protein name**
CDC27	cell division cycle 27	-2,894	0,003	EPN1	epsin 1	-3,188	0,004	PKN1	protein kinase N1
AUTS2	activator of transcription and developme	-2,638	0,047	PKN1	protein kinase N1	-2,668	0,001	CIC	capicua transcriptional repressor

Preprints (www.preprints.org) | NOT PEER-REVIEWED | Posted: 12 May 2023 doi:10.20944/preprints202305.0896.v1

	ntal regulator								
DMXL2	Dmx like 2	-2,150	0,009	PITPNM1	phosphatidylinositol transfer protein membrane associated 1	-2,640	0,029	TOP2B	DNA topoisomerase II beta
PICALM	phosphatidylinositol binding clathrin assembly protein	-2,100	0,045	MAP7D1	MAP7 domain containing 1	-2,530	0,039	CCDC88A	coiled-coil domain containing 88A
TRAF7	TNF receptor associated factor 7	-2,100	0,007	MTMR2	myotubularin related protein 2	-2,225	0,029	PBRM1	polybromo 1
PARD3B	par-3 family cell polarity regulator beta	-2,069	0,005	GRK1	G protein-coupled receptor kinase 1	-2,180	0,023		
AMPH	amphiphysin	-2,051	0,004	PCBP1	poly(rC) binding protein 1	-2,144	0,033		
ATG16L1	autophagy related 16 like 1	-2,006	0,008	JPT1	Jupiter microtubule associated homolog 1	-2,115	0,034		
RNF34	ring finger protein 34	-1,980	0,007	EPB41	Protein 4.1 isoform 2	-2,023	0,049		
ACIN1	apoptotic chromatin condensation inducer 1	-1,934	0,023	GPHN	Gephyrin	-1,836	0,031		
SYN3	synapsin III	-1,759	0,048	PPP6R2	protein phosphatase 6 regulatory subunit 2	-1,826	0,010		
DPY30	dpy-30 histone methyltransferase	-1,759	0,050	FLNB	filamin B	-1,762	0,009		

Preprints (www.preprints.org) | NOT PEER-REVIEWED | Posted: 12 May 2023 doi:10.20944/preprints202305.0896.v1

	complex regulatory subunit								
ZNF687	zinc finger protein 687	-1,747	0,013	RNF20	ring finger protein 20	-1,747	0,040		
CTBP2	C-terminal binding protein 2	-1,736	0,036	TSC22D1	TSC22 domain family member 1	-1,602	0,016		
CCDC88A	coiled-coil domain containing 88A	-1,696	0,023	LIN37	lin-37 DREAM MuvB core complex component	-1,595	0,002		
SMPD3	sphingomyelin phosphodiesterase 3	-1,666	0,000	CIC	capicua transcriptional repressor	-1,480	0,040		
NKTR	natural killer cell triggering receptor	-1,583	0,024	SLC20A2	solute carrier family 20 member 2	-1,416	0,048		
NONO	non-POU domain containing octamer binding	-1,554	0,014	PRKG1	protein kinase cGMP-dependent 1	-1,387	0,019		
RBM8A	RNA binding motif protein 8A	-1,509	0,033	ARHGAP21	Rho GTPase activating protein 21	-1,385	0,041		
SNX2	sorting nexin 2	-1,500	0,014	PABIR1	PP2A Aalpha (PPP2R1A) and B55A (PPP2R2A) interacting phosphatase regulator 1	-1,356	0,039		

Preprints (www.preprints.org) | NOT PEER-REVIEWED | Posted: 12 May 2023 doi:10.20944/preprints202305.0896.v1

Table 2. Lists of proteins showing increased phosphorylation after PKG inhibition for either 2 hours (left column) or 4 hours (center column), whereas the right column shows proteins that showed increased phosphorylation at both time points. Note that the left and center columns only show the 20 proteins with highest fold change for 2 hours and 4 days, respectively. The total number of proteins with increased phosphorylation was 83 and 130 after 2 hours and 4 days PKG inhibition, respectively. Full lists of all proteins/peptides with increased phosphorylation are found in Supplementary Tables S1 and S2.

Proteins with increased phosphorylation after PKG inhibition									
Top 20 after 2 hours				**Top 20 after 4 days**				**Appearing in both**	
Gene symbol	Protein name	Fold Change	P-value	Gene symbol	Protein name	Fold Change	P-value	Gene symbol	Protein name
HNRNPUL1	heterogeneous nuclear ribonucleoprotein U like 1	3,343	0,006	MAP1B	microtubule associated protein 1B	3,674	0,009	HNRNPUL1	heterogeneous nuclear ribonucleoprotein U like 1
EEF1B2	eukaryotic translation elongation factor 1 beta 2	2,593	0,002	LGALS12	galectin 12	2,279	0,016	PALM2AKAP2	PALM2 and AKAP2 fusion
HNRNPU	heterogeneous nuclear ribonucleoprotein U	2,242	0,035	HNRNPUL1	heterogeneous nuclear ribonucleoprotein U like 1	2,138	0,006	DLG1	discs large MAGUK scaffold protein 1
GTPBP1	GTP binding protein 1	2,165	0,012	NR5A1	nuclear receptor subfamily 5 group A member 1	2,128	0,001	SEPTIN4	septin 4
MAP4	microtubule associated protein 4	2,161	0,026	GTF2F1	general transcription factor IIF subunit 1	2,115	0,015	MAP1B	microtubule associated protein 1B
VPS53	VPS53 subunit of GARP complex	2,083	0,037	SRRM2	serine/arginine repetitive matrix 2	2,041	0,000	HNRNPU	heterogeneous nuclear ribonucleoprotein U
NES	nestin	1,725	0,048	RBSN	rabenosyn, RAB effector	2,006	0,026	MCM7	minichromosome maintenance complex component 7
LARP1	La ribonucleo	1,650	0,035	TPD52L2	TPD52 like 2	1,946	0,010	ATF7IP	activating transcriptio

Preprints (www.preprints.org) | NOT PEER-REVIEWED | Posted: 12 May 2023 doi:10.20944/preprints202305.0896.v1

	protein 1, translational regulator								n factor 7 interacting protein
CDK13	cyclin dependent kinase 13	1,621	0,024	VSX2	visual system homeobox 2	1,945	0,028	MAP4	microtubule associated protein 4
AFDN	afadin, adherens junction formation factor	1,323	0,012	RBM12	RNA binding motif protein 12	1,915	0,008	ANK2	ankyrin 2
PXN	paxillin	1,284	0,001	DZIP3	DAZ interacting zinc finger protein 3	1,897	0,021	SRRM1	serine and arginine repetitive matrix 1
RCOR1	REST corepressor 1	1,275	0,025	ABLIM1	actin binding LIM protein 1	1,842	0,031	KIAA0930	KIAA0930
RUNX1T1	RUNX1 partner transcriptional co-repressor 1	1,230	0,039	PITPNM2	phosphatidylinositol transfer protein membrane associated 2	1,827	0,028	CCDC88A	coiled-coil domain containing 88A
HTATSF1	HIV-1 Tat specific factor 1	1,199	0,016	ELF2	E74 like ETS transcription factor 2	1,778	0,024	CTBP2	C-terminal binding protein 2
ZC3H6	zinc finger CCCH-type containing 6	1,143	0,017	BICRAL	BRD4 interacting chromatin remodeling complex associated protein like	1,771	0,047	MAP2	microtubule associated protein 2
BRAF	B-Raf proto-oncogene, serine/threonine kinase	1,127	0,031	PALM2AKAP2	PALM2 and AKAP2 fusion	1,761	0,040	RERE	arginine-glutamic acid dipeptide repeats
BASP1	brain abundant membrane attached signal protein 1	1,122	0,000	DNAJC5	DnaJ heat shock protein family (Hsp40) member C5	1,707	0,028		

Preprints (www.preprints.org) | NOT PEER-REVIEWED | Posted: 12 May 2023 doi:10.20944/preprints202305.0896.v1

PLCL2	phospholipase C like 2	1,086	0,030	PACS2	phosphofurin acidic cluster sorting protein 2	1,705	0,029		
SPHK2	sphingosine kinase 2	1,012	0,004	CCNL1	cyclin L1	1,650	0,002		
SEPTIN 4	septin 4	0,987	0,047	EIF4EBP1	eukaryotic translation initiation factor 4E binding protein 1	1,647	0,019		

Table 3. Kinases with proposed altered activities after various lengths of PKG inhibition, as indicated by the upstream kinase tool. The four columns give kinases that appear in both of the two situations indicated at the head of each column. Full lists of all proposed kinase alterations are found in Supplementary Tables S3 and S4.

Decreased after 2 hours/ Decreased after 4 days	Increased after 2 hours /Increased after 4 days	Decreased after 2 hours /Increased after 4 days	Increased after 2 hours /Decreased after 4 days
CDK1	CSNK1E	CDK2	MAPK3
PRKACA	MAP2K7	PRKAA2	MAPK1
	MAP2K4	MAP3K7	PRKCE
	MAP3K5	CDK7	
	CSNK2A1		
	CSNK2A2		
	CSNK1E		
	BCR		
	MAPK8		
	MTOR		
	MAPK14		

3.2. Potential cGMP-PKG dependent biological pathways

To address the biological pathways that the cGMP-PKG dependent substrates were involved in, a protein annotation in Kyoto Encyclopedia of Genes and Genomes (KEGG), with the targets mentioned above, was performed. Proteins with decreased phosphorylated sites after PKG inhibition were annotated in RNA transport, Spliceosome and Rap1 signaling pathway (Figure 2A). A part of these down-regulated sites after PKG inhibition, such as the sites in protein kinase cGMP-dependent 1 (PKG1), general transcription factor IIi (GTF2I) and protein phosphatase 1 catalytic subunit alpha (PPP1CA), were involved in the cGMP-PKG pathway. This supported that PKG signaling in explants were appropriately inhibited during culturing. By contrast, the proteins of the increased phosphorylation were mostly related to pathways connected with proteoglycans, ErbB signaling and tight junctions (Figure 2B).

Preprints (www.preprints.org) | NOT PEER-REVIEWED | Posted: 12 May 2023 doi:10.20944/preprints202305.0896.v1

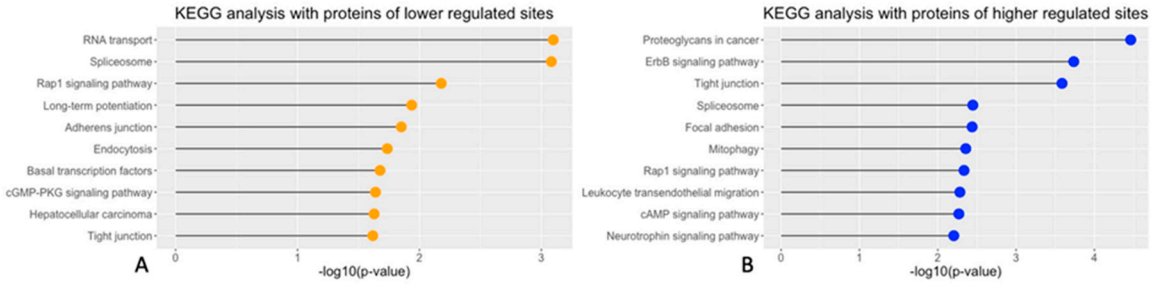

Figure 2. KEGG analyses of pathways connected with the observed phosphorylation changes. A: Top 10 significant biological pathways enriched in the KEGG analysis and thus connected with proteins having decreased phosphorylated sites. B: Top 10 significant biological pathway for sites with increased phosphorylation.

3.3. Upstream kinase analysis

To predict the upstream kinases for the altered phosphorylations identified above, the regulated phosphoproteins were analyzed via annotation to the online tool Phosphomatics V2 (https://phosphomatics.com/). The outcomes are given as kinome trees (Figure 3A and 3B) and as lists (Supplementary Tables S3 and S4). For the 2 hours treatment, the algorithms suggested a total of 66 potential upstream kinases, 32 with decreased activity, and 34 with increased activity (Figure 3A, Supplementary Table S3). Among these, 7 kinases in the category of proposed decreased activity, and 11 of the increased ones, phosphorylate their substrates in a site-specific manner (Supplementary Table S3).

For the 4 days treatment, the number of suggested upstream kinases reached 68, of which 8 had decreased activity, and 60 had increased activity (Figure 3B, Supplementary Table S4). In this case the site-specific ones were represented by 3 and 5 kinases of those with proposed decreased and increased activity, repectively (Supplementary Table S4). Table 3 summarizes the kinases that had a consistent reaction to the treatment between the two timepoints. Two kinases gave indications of having reduced activity after both timepoints, namely cyclin dependent kinase 1 (CDK1) and cAMP-dependent protein kinase catalytic subunit alpha (PRKACA), whereas 10 kinases came up as having increased activity at both timepoints. Of the latter, 4 kinases were related to the MAPK family (Table 3). There were also some kinases who displayed opposite reactions to the treatment after 2 hours and 4 days (Table 3). These are not considered further in this report.

Preprints (www.preprints.org) | NOT PEER-REVIEWED | Posted: 12 May 2023 doi:10.20944/preprints202305.0896.v1

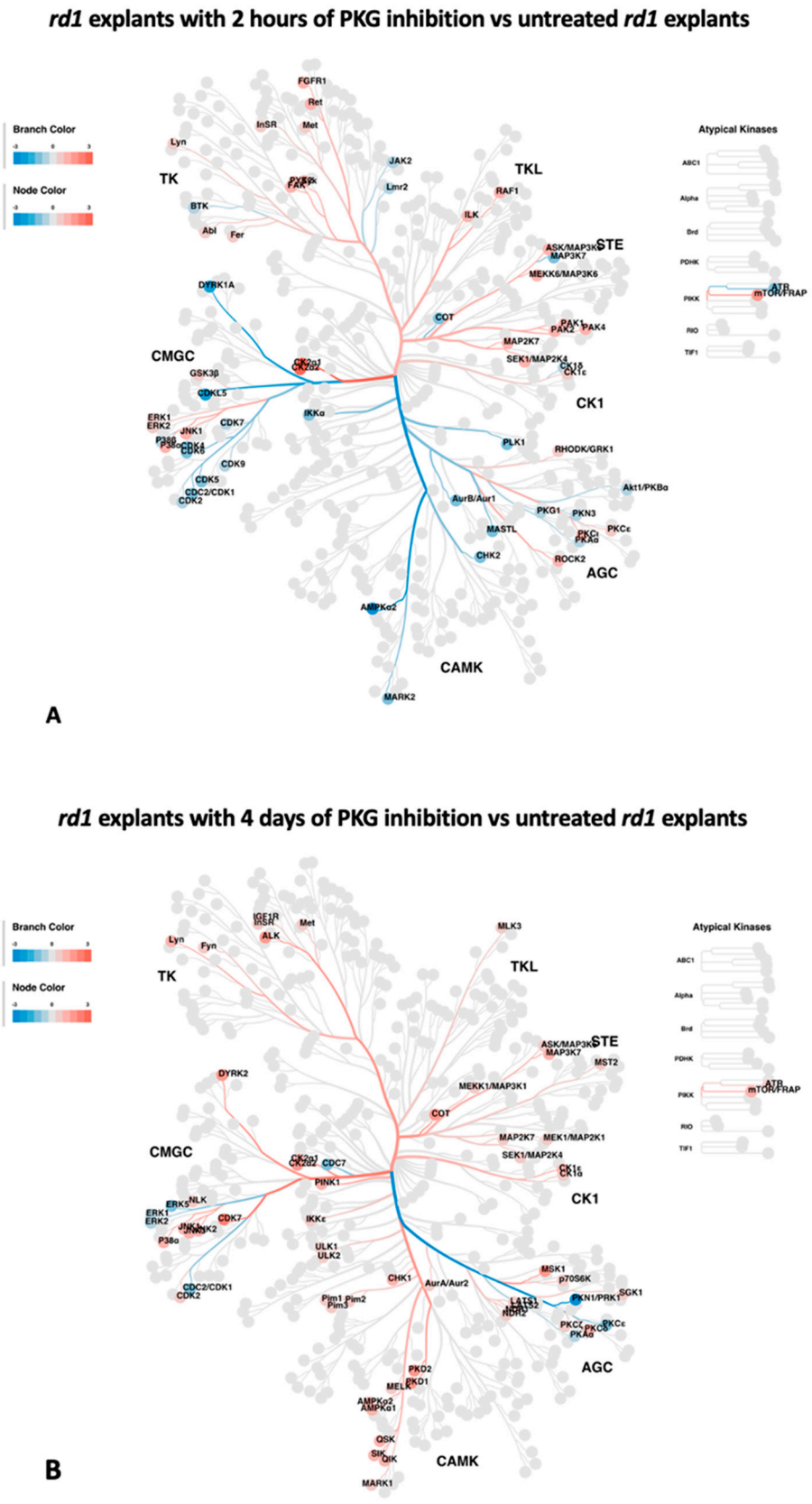

Figure 3. Potential altered kinases, as indicated by the upstream kinase tool, are visualized as kinome phylogenetic trees. The branch and node colors are encoded by Fold Change, with values < 0 (in blue) and > 0 (in red) representing kinase activity as decreased or increased, respectively, in rd1 explants with PKG inhibition compared to untreated rd1 explants. A: Kinome phylogenetic tree with potential kinases altered in rd1 with PKG inhibition for 2 hours. B. Kinome phylogenetic tree with potential kinases altered in rd1 with PKG inhibition for 4 days.

 doi:10.20944/preprints202305.0896.v1

3.4. Selection of RAF-1 for further validation

To gain more insights in the cGMP-PKG network, one target was selected from the upstream kinase analysis for further validation. Since the abnormally high level of cGMP in the photoreceptors is regarded as a disease driver of retinal degeneration [21], we assumed that photoreceptor-specific proteins have an essential role in the retinal dysfunction. For this purpose the RAF proto-oncogene serine/threonine-protein kinase (RAF1) was selected for additional analysis. As mentioned above, several of the upstream kinases with increased activities belonged to the MAPK family. The rationale for selecting RAF is thus that MAPK1 is expressed in photoreceptors and is linked to photoreceptor death, at any rate in Drosophila [22], and also that RAS and its downstream pathway component RAF1 are required to satisfy photoreceptor differentiation [23]. In addition, RAF1 was proposed as having higher kinase activity after 2 hours of PKG inhibition (Supplementary Table S3). Therefore, as part of the well-established Ras/Raf-1/MAPK1 signaling, the role of RAF1 during retinal degeneration and its connection with cGMP-PKG system was of interest to analyse further.

To see whether RAF1 is specifically expressed within photoreceptors, retinas from either *rd1* or wt animals were immunostained for RAF1. In wt RAF1 was expressed pre-dominantly in the photoreceptor segments. This was also true for *rd1*, which in addition displayed elevated RAF1 staining in many parts of the *rd1* outer nuclear layer (ONL), where the photoreceptor cell bodies and processes reside (Figure 4A, B and C). This supports that RAF1 can be seen as a relatively photoreceptor-specific kinase and that it could be involved in photoreceptor degeneration.

Next, the potential link between RAF1 expression and the cGMP-PKG system was investigated at the histological level. This was achieved via pharmacological PKG inhibition in retinal explants during culturing (the same culturing paradigms as above), followed by analysis of possible RAF1 alterations in photoreceptors after treatment. Figure 5 shows that the RAF1 expression was higher in the ONL after PKG inhibition, regardless of the different lengths of treatment.

To see if the change in RAF1 expression was in any way also reflected in the phosphorylation state of RAF1, the PLA technique for the combination of RAF1 protein and phosphorylated serine [24] to study the RAF1 phosphorylation profile was applied. The PLA uses antibodies against two different antigens, as well as certain secondary antibodies containing complimentary"primers" of a reaction product. If the two antigens are in close proximity (<40 nm) the method then allows a reaction product to be formed. Thus, if the RAF antibody is in close contact with the phosphoserine antibody, it is likely that both antibodies sit on the same protein, namely RAF1, and thus identify phosphorylated RAF1. We focused on the RAF1 phosphorylation in ONL, since RAF1 was higher expressed in the *rd1* ONL (Figure 4) and found an increased level of PLA signal within the ONL of *rd1* (Figure 6). This indicated a higher extent of RAF1 phosphorylation in retinas undergoing degeneration.

Next question was if the RAF1 phosphorylation could be affected by manipulation of the cGMP-PKG system during culturing. We observed that RAF1 phosphorylation was higher in the ONL of retinal explants being treated with PKG inhibitor for 2 hours (Figure 7A, B, E), while no difference to the untreated counterpart was noticed after 4 days of treatment (Figure 7C, D, E). This was consistent with our discovery in the upstream kinase analysis, that a higher RAF1 activity was identified in explants with 2 hours of PKG inhibition but not in the 4 days treatment (Figure 3A and 3B, Supplementary Tables S3 and S4). Note that the overwhelming amount of the phosphorylated RAF1 resided in the ONL and the photoreceptor segments.

Preprints (www.preprints.org) | NOT PEER-REVIEWED | Posted: 12 May 2023 doi:10.20944/preprints202305.0896.v1

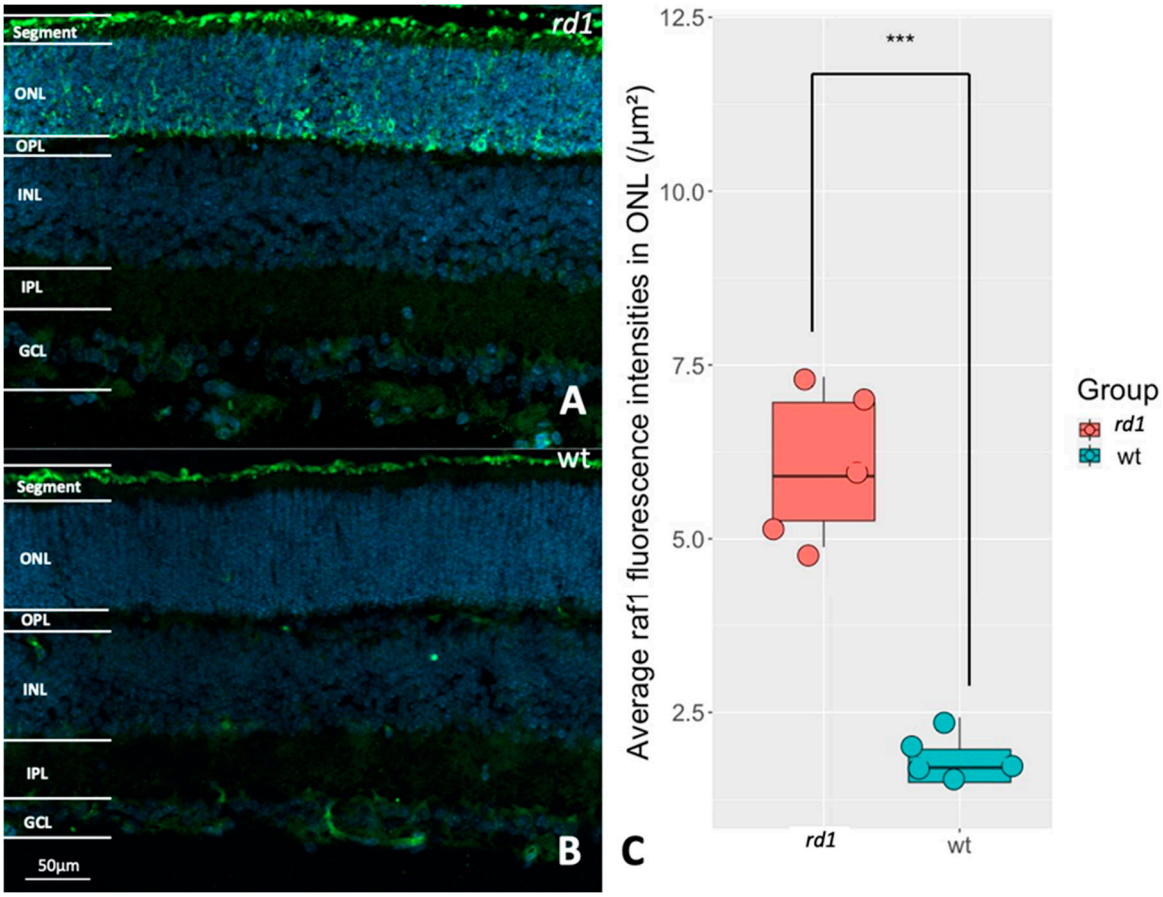

Figure 4. Evaluation of RAF1 expression in rd1 and wt retinas. A: Immunostaining of RAF1 (green) in a P11 rd1 retina. B: Immunostaining of RAF1 (green) in a P11 wt retina. DAPI (blue) was used as nuclear counterstain. C: The box chart shows the comparison of RAF fluorescence intensities within the outer nuclear layer (ONL) between rd1 (n=5) and wt (n=5), ***$p < 0.001$.

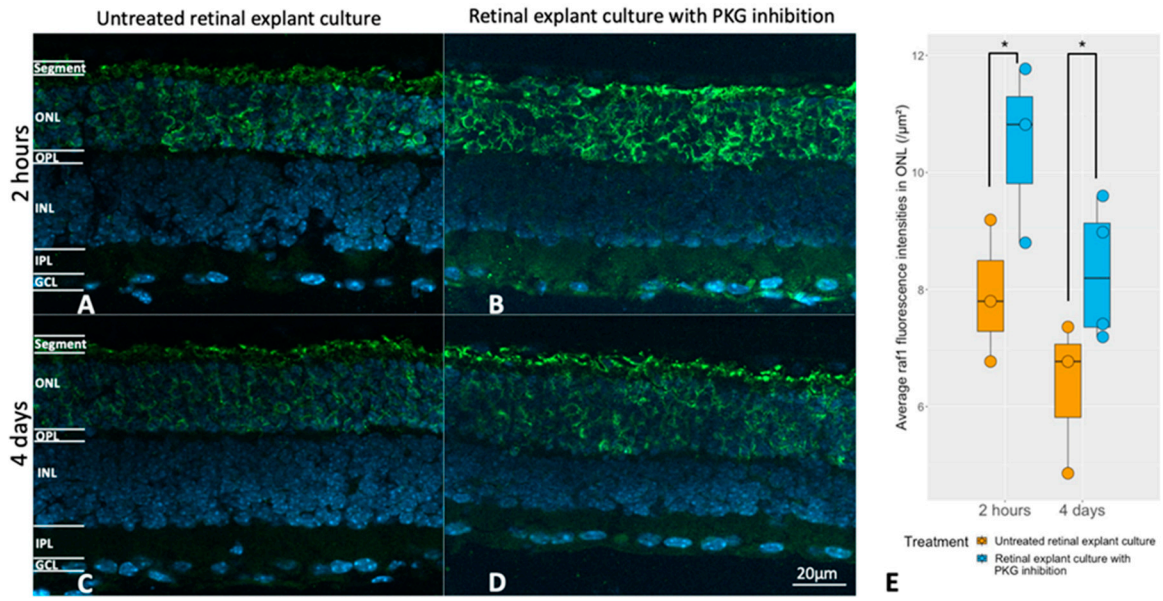

Figure 5. Evaluation of the relation between the cGMP-PKG system and RAF1 expression. Retinal explants from rd1 were treated with 50 µM Rp-8-Br-PET-cGMPS (PKG inhibitor) for 2 hours (n=3) and their untreated counterparts (n=3), or the same compound in the same concentration for 4 days (n=4) and their untreated controls (n=3). A and B represent RAF1 (green) immunostaining in untreated retinal explants and their counterparts with 2 hours of PKG inhibition. C and D represent immunostaining of RAF1 in untreated retinal explants and their counterparts with 4 days of PKG

Preprints (www.preprints.org) | NOT PEER-REVIEWED | Posted: 12 May 2023 doi:10.20944/preprints202305.0896.v1

inhibition. DAPI (blue) was used as nuclear counterstain. E: The box chart compares RAF fluorescence intensities within the ONL between untreated explants and peers with PKG inhibitor in different treatment lengths. *p < 0.05.

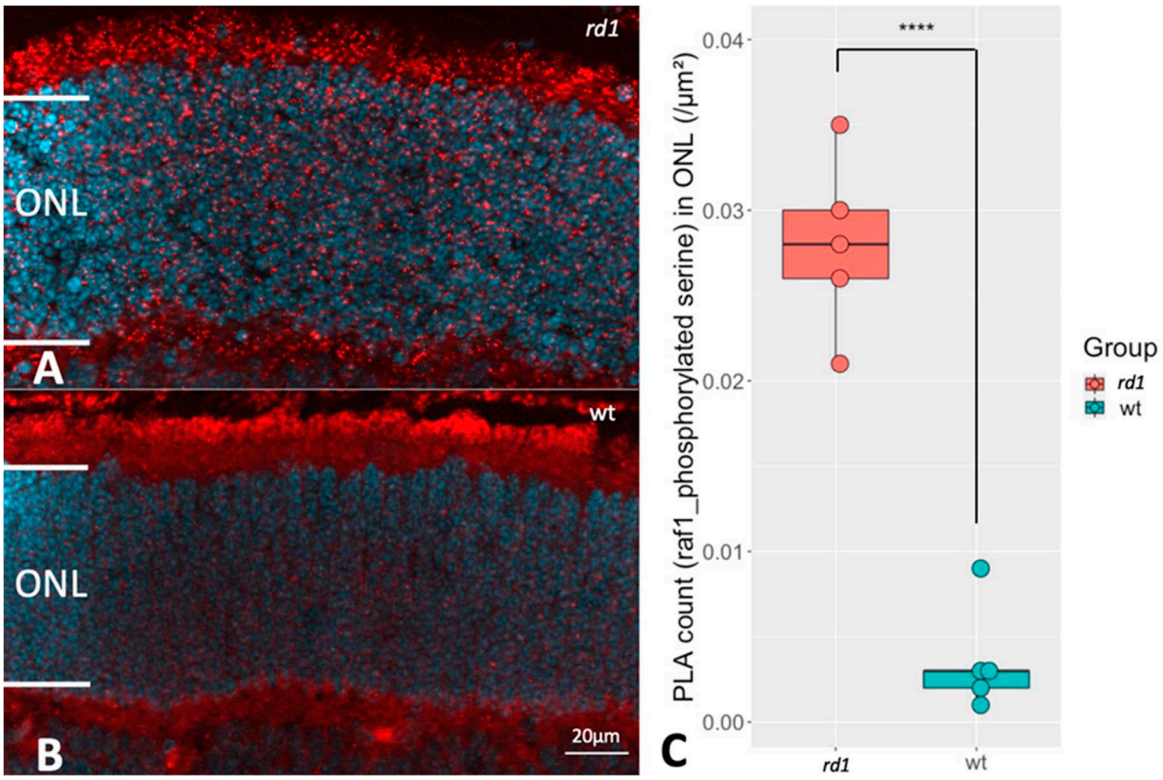

Figure 6. Comparison of RAF1 phosphorylation between rd1 and wt retinas. The proximity ligation assay (PLA) punctuations indicate that RAF1 is in proximity with phosphoserine, which reveals the RAF1 phosphorylation profile. A and B represent PLA punctuations (RAF1 and phosphorylated serine) in ONL from rd1 and wt, respectively. DAPI (blue) was used as nuclear counterstain C: The box chart shows the comparison of PLA counts in ONL of retinas from rd1 (n=5) and wt (n=5). ****p < 0.0001.

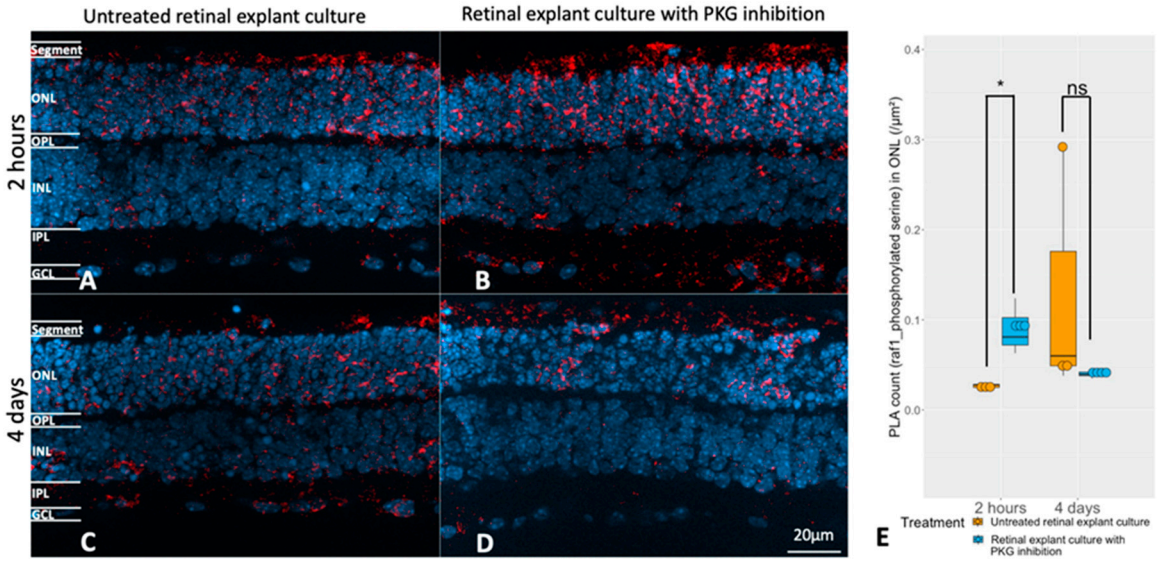

Figure 7. Evaluation of the relation between the cGMP-PKG system and RAF1 phosphorylation. Retinal explants from rd1 were treated with 50 µM Rp-8-Br-PET-cGMPS (PKG inhibitor) for 2 hours (n=3) and their untreated counterparts (n=3), or the same compound in the same concentration for 4 days (n=4) and their untreated controls (n=3). A and B represent PLA (red, RAF1 and phosphorylated

 doi:10.20944/preprints202305.0896.v1

serine) in untreated retinal explants and the counterparts with 2 hours PKG inhibition. C and D represent PLA punctuations in untreated retinal explants and the counterparts with 4 days PKG inhibition. DAPI (blue) was used as nuclear counterstain. E: The box chart shows the comparison of PLA counts within ONL between untreated retinal explants controls and peers with PKG inhibitor in different length of treatment (n=3-4). *$p < 0.05$.

4. Discussion

MS-based phosphoproteomics techniques has been extensively applied in biological research, including in retinal studies [25]. Technically, one option is to apply immunoprecipitation for phosphoprotein enrichment prior to MS detection. However, due to the limitation of commercially phospho-selective antibodies, this approach has not provided promising results in phosphoprotein enrichment [26], and is therefore unsuitable for high throughput phosphoproteomic study. Another widely applied strategy is the use of immobilized metal affinity chromatography, as in the current study. Though the non-specificity has been noticed for this method, the continuous optimization of the protocol has made it frequently applied in phosphoproteomic research [27] including here.

Our study has three clear outcomes: 1) It identified potential retinal PKG substrates that could be involved in retinal degeneration, 2) it gave information on the kinase and pathway networks in operation during the degenerative events, and 3) it showed a correlation between the cGMP-PKG system and the RAS/RAF/MAPK/ERK pathway in this situation.

The upstream kinase and KEGG analyses both picked up PKG or the cGMP-PKG signaling pathway as being affected by the treatment, which corroborated the usefulness of the approach. In addition, the two treatment regimes, *i.e.* 2 hours or 4 days of PKG inhibition, gave data on proteins whose phosphorylation was decreased as well as such that displayed increased phosphorylation in either or both of these regimes.

The assumption that increased phosphorylation by PKG is part of the degeneration mechanism, makes the proteins with reduced phosphorylation at both time points of PKG inhibition particularly interesting with respect to a pathologic involvement. Among the five proteins of this category, we noticed DNA Topoisomerase II Beta (TOP2B) and capicua transcriptional repressor (CIC). Deletion of TOP2B harms photoreceptors [28], and TOP2B mRNA was in our previous transcriptome study reduced by PKG inhibition in *rd1* explants [17]. Given that TOP2B phosphorylation affects its functions [29], one may consider that PKG-dependent over-phosphorylation of TOP2B leads to dysfunctional transcription [30], which could affect the photoreceptors' wellbeing. Likewise, our transcriptome study also connected CIC with the cGMP-PKG system [17]. CIC is a transcriptional repressor, with an involvement in neurodegeneration [31] and in nervous system differentiation. CIC has a connection also with the ataxin-1 like protein (ATXN1L), in the sense that they in concert with yet other proteins (ETS transcription factors) may act to modulate the sensitivity of the MAPK pathway [32]. It is in this context interesting that the phosphorylation of ATXN1L was reduced in the 2 hours PKG inhibition experiment (Supplementary Table S1). Taken together, there is reason to keep TOP2B and CIC as candidates for links between PKG activity and events during retinal degeneration.

Proteins that instead showed persistent *increased* phosphorylation after PKG inhibition are, by contrast, more likely to be dependent on kinases under direct or indirect negative regulation by PKG, and were represented by as many as 16 proteins. Some deserve to be mentioned here, such as ankyrin 2 (ANK2), with a possible role in maintaining ion balance, via anchoring of ion transporters to the photoreceptor cell membrane [33]. Proteins of the microtubule-associated protein (MAP) family, including MAP1B, MAP2 and MAP4, were also seen. MAPs could be critical for photoreceptors and at least one of these may associate with retinal degeneration [34,35].

The upstream kinase analysis indicated an integration of the cGMP-PKG pathway with other kinases, of which those with potentially lower activity after 2 hours and 4 days of treatment included CDK1 and protein kinase cAMP-activated catalytic subunit alpha (PRKACA). For the CDK1, we recently demonstrated its expression in degenerating *rd1* photoreceptors, as well as that this was reduced by PKG inhibition [36]. Together with our present observation that lower CDK1 activities

were predicted already 2 hours and 4 days after PKG was inhibited, a possible interpretation would be that CDK1 expression is somehow affected by a cGMP-PKG regulated phosphorylation.

Several kinases with potential higher activities after PKG inhibition were from the mitogen-activated protein kinase (MAPK) family. MAPK signaling, particularly via the activation of the p38 MAPK subclass, has been shown to have neuroprotective effects in degenerating photoreceptors [37]. MAPK14 belongs to this subclass and was suggested to have increased activity after both 2 hours and 4 days of PKG inhibition. The upstream kinase analysis moreover pointed to higher activities of two dual-specificity MAPKs, termed MAP kinase kinases (MAP2K) and mitogen activated protein kinase kinase kinase (MAP3K), and at least MAP2K is known as a p38 MAPK regulator responsible for its activation [38]. The MAPKs therefore appear connected with the degeneration, including in a PKG related way.

The RAS/RAF1/MAPK/ERK pathway with its diverse biological functions is one of the most extensively studied signal transduction routes [39] and here we provide insights into how RAF1 may connect with retinal degeneration. In wt retinas the predominant expression of RAF1 was in the segments, pointing to it being a photoreceptor specific kinase. The increased expression and phosphorylation of RAF1 in the *rd1* compared to wt ONL revealed in turn that it may participate in the degeneration of the photoreceptors, as did the above mentioned suggested increased activation of several MAPKs.

However, neither its increased expression nor the increased phosphorylation specifies whether RAF1 works for or against the degeneration. Our results of PKG inhibition in *rd1* explants provided more clues, though, since RAF1 expression increased after both lengths of treatment and more phosphorylated RAF1 was seen after 2 hours of PKG inhibition. Given that retinal degeneration benefits from such PKG inhibition [8,9], RAF1 may exert neuroprotective effects during photoreceptor death. Had it been the opposite, that the expression and phosphorylation state of RAF1 drives the degeneration, both these parameters would have been expected to decrease after PKG inhibition. Yet the situation is not straightforward, since phosphorylation of RAF1 may lead to either its inhibition or activation, depending on the actual serine site [40], which we were not able to discriminate between here. While highly speculative, the suggested activation of RAF1 in the upstream kinase analysis could mean that the degeneration initiates a protective program involving RAF1 activity, but that PKG counteracts the same by blocking the activity, probably via other kinase or even phosphatase activities.

In conclusion, our study shows an intricate pattern of changes with respect to protein phosphorylations after inhibition of PKG. It appears likely that several of these results, including those connected to the RAS/RAF1/MAPK/ERK pathway, relate to the yet unclarified mechanisms of inherited retinal degeneration and as such will aid in designing future investigations in this area.

Acknowledgments: This study was sponsored by the European Union's Horizon 2020 research and innovation programme under the Marie Sklodowska-Curie grant agreement No 765441 (transMed; H2020-MSCA-765441), The Stiftelsen Hedda och John Forssmans No 40642, Stiftelsen för Synskadade i f.d. Malmöhus län, Kronprinsessan Margaretas Arbetsnämnd för synskadade, Carmen och Bertil Regnérs Stiftelse för forskning inom området ögonsjukdomar, and Ögonfonden. We would like to thank the Center for Translational Proteomics at Medical Faculty, Lund University, Sweden for insightful discussions.

Ethics statement: All animal experiments and procedures adhered to the permit that was approved by Malmö - Lunds djurförsöksetiska nämnd, with the reference coded as #M92-15 and 02124/2020.

Conflict of Interest: P.E. has financial interest in the company Mireca Medicines, which intends to forward clinical testing of the compound used here for PKG inhibition. J.Z. and C.W. have no conflicts of interest.

References

1. De Silva, S.R. et al. (2021) "The X-linked retinopathies: Physiological insights, pathogenic mechanisms, phenotypic features and novel therapies," Progress in Retinal and Eye Research, 82, p. 100898.
2. He, Y., Zhang, Y. and Su, G., 2015. Recent Advances in Treatment of Retinitis Pigmentosa. Current Stem Cell Research & Therapy, 10(3), pp.258-265.

3. Russell, S., Bennett, J., Wellman, J. A., Chung, D. C., & et al. (2017). Efficacy and safety of voretigene neparvovec (AAV2-hRPE65v2) in patients with RPE65-mediated inherited retinal dystrophy: a randomised, controlled, open-label, phase 3 trial. The Lancet, 390(10097), 849–860.
4. Campochiaro, P.A. (2019) "Mechanism of cone cells death in retinitis pigmentosa," Acta Ophthalmologica, 97(S263).
5. Farber, D. and Lolley, R., 1974. Cyclic Guanosine Monophosphate: Elevation in Degenerating Photoreceptor Cells of the C3H Mouse Retina. Science, 186(4162), pp.449-451.
6. Pennesi, M.E. et al. (2012) "Long-term characterization of retinal degeneration inrd1andrd10mice using spectral domain optical coherence tomography," Investigative Opthalmology & Visual Science, 53(8), p. 4644.
7. Strettoi, E. et al. (2003) "Remodeling of second-order neurons in the retina of RD/RD Mutant Mice," Vision Research, 43(8), pp. 867–877. Available at: https://doi.org/10.1016/s0042-6989(02)00594-1.
8. Paquet-Durand, F., Hauck, S., van Veen, T., Ueffing, M. and Ekström, P. 2009. PKG activity causes photoreceptor cell death in two retinitis pigmentosa models. Journal of Neurochemistry 108: 796-810
9. Vighi, E., Trifunović, D., Veiga-Crespo, P., Rentsch, A., Hoffmann, D., Sahaboglu, A., Strasser, T., Kulkarni, M., Bertolotti, E., van den Heuvel, A., Peters, T., Reijerkerk, A., Euler, T., Ueffing, M., Schwede, F., Genieser, H., Gaillard, P., Marigo, V., Ekström, P. and Paquet-Durand, F. (2018). Combination of cGMP analogue and drug delivery system provides functional protection in hereditary retinal degeneration. Proceedings of the National Academy of Sciences, 115(13), pp.E2997-E3006.
10. Hofmann, F., Feil, R., Kleppisch, T. and Schlossmann, J. (2006). Function of cGMP-Dependent Protein Kinases as Revealed by Gene Deletion. Physiological Reviews, 86(1), pp.1-23.
11. Choi, C., Sellak, H., Brown, F. and Lincoln, T. (2010). cGMP-dependent protein kinase and the regulation of vascular smooth muscle cell gene expression: possible involvement of Elk-1 sumoylation. American Journal of Physiology-Heart and Circulatory Physiology, 299(5), pp.H1660-H1670.
12. Pilz, R. and Casteel, D. (2003). Regulation of Gene Expression by Cyclic GMP. Circulation Research, 93(11), pp.1034-1046.
13. Fajardo, A., Piazza, G. and Tinsley, H., 2014. The Role of Cyclic Nucleotide Signaling Pathways in Cancer: Targets for Prevention and Treatment. Cancers, 6(1), pp.436-458.
14. Butt, E., Pöhler, D., Genieser, H., Huggins, J. and Bucher, B. 1995. Inhibition of cyclic GMP-dependent protein kinase-mediated effects by (Rp)-8-bromo-PET-cyclic GMPS. Br. J. Pharmacol. 116: 3110-3116.
15. Rapoport, R., Draznin, M. and Murad, F., 1982. Sodium nitroprusside-induced protein phosphorylation in intact rat aorta is mimicked by 8-bromo cyclic GMP. Proceedings of the National Academy of Sciences, 79(21), pp.6470-6474.
16. Schwede, F., Maronde, E., Genieser, H. and Jastorff, B. (2000). Cyclic nucleotide analogs as biochemical tools and prospective drugs. Pharmacology & Therapeutics, 87(2-3), pp.199-226.
17. Zhou, J., Rasmussen, M. and Ekström, P., 2021. cGMP-PKG dependent transcriptome in normal and degenerating retinas: Novel insights into the retinitis pigmentosa pathology. Experimental Eye Research, 212, p.108752.
18. Mann, M., Ong, S., Grønborg, M., Steen, H., Jensen, O. and Pandey, A., 2002. Analysis of protein phosphorylation using mass spectrometry: deciphering the phosphoproteome. Trends in Biotechnology, 20(6), pp.261-268.
19. Sanyal, S.; Bal, A.K. Comparative light and electron microscopic study of retinal histogenesis in normal and rd mutant mice. Z. Anat. Entwicklungs. 1973, 142, 219–238.
20. Hornbeck, P., Zhang, B., Murray, B., Kornhauser, J., Latham, V. and Skrzypek, E., 2014. PhosphoSitePlus, 2014: mutations, PTMs and recalibrations. Nucleic Acids Research, 43(D1), pp.D512-D520.
21. Power, M., Das, S., Schütze, K., Marigo, V., Ekström, P. and Paquet-Durand, F., 2020. Cellular mechanisms of hereditary photoreceptor degeneration – Focus on cGMP. Progress in Retinal and Eye Research, 74, p.100772.
22. Roignant, J. and Treisman, J., 2010. Exon Junction Complex Subunits Are Required to Splice Drosophila MAP Kinase, a Large Heterochromatic Gene. Cell, 143(2), pp.238-250.
23. Dhillon, A., Meikle, S., Peyssonnaux, C., Grindlay, J., Kaiser, C., Steen, H., Shaw, P., Mischak, H., Eychène, A. and Kolch, W., 2003. A Raf-1 Mutant That Dissociates MEK/Extracellular Signal-Regulated Kinase Activation from Malignant Transformation and Differentiation but Not Proliferation. Molecular and Cellular Biology, 23(6), pp.1983-1993.

24. Weibrecht, I., Leuchowius, K., Clausson, C., Conze, T., Jarvius, M., Howell, W., Kamali-Moghaddam, M. and Söderberg, O., 2010. Proximity ligation assays: a recent addition to the proteomics toolbox. Expert Review of Proteomics, 7(3), pp.401-409.
25. Cehofski, L.J. et al. (2014) "Analytical platforms in vitreoretinal proteomics," Bioanalysis, 6(22), pp. 3051–3066. Available at: https://doi.org/10.4155/bio.14.227.
26. Grønborg, M. et al. (2002) "A mass spectrometry-based proteomic approach for identification of serine/threonine-phosphorylated proteins by enrichment with phospho-specific antibodies," Molecular & Cellular Proteomics, 1(7), pp. 517–527.
27. Fíla, J. and Honys, D. (2011) "Enrichment techniques employed in phosphoproteomics," Amino Acids, 43(3), pp. 1025–1047.
28. Li, Y., Hao, H., Swerdel, M., Cho, H., Lee, K., Hart, R., Lyu, Y. and Cai, L., 2017. Top2b is involved in the formation of outer segment and synapse during late-stage photoreceptor differentiation by controlling key genes of photoreceptor transcriptional regulatory network. Journal of Neuroscience Research, 95(10), pp.1951-1964.
29. Bedez, C., Lotz, C., Batisse, C., Broeck, A., Stote, R., Howard, E., Pradeau-Aubreton, K., Ruff, M. and Lamour, V., 2018. Post-translational modifications in DNA topoisomerase 2α highlight the role of a eukaryote-specific residue in the ATPase domain. Scientific Reports, 8(1).
30. Lang, A., Mirski, S., Cummings, H., Yu, Q., Gerlach, J. and Cole, S., 1998. Structural organization of the human TOP2A and TOP2B genes. Gene, 221(2), pp.255-266.
31. Jiménez G, Shvartsman SY, Paroush Z. The Capicua repressor--a general sensor of RTK signaling in development and disease. J Cell Sci. 2012 Mar 15;125(Pt 6):1383-91.
32. Wang B, Krall EB, Aguirre AJ, Kim M, Widlund HR, Doshi MB, Sicinska E, Sulahian R, Goodale A, Cowley GS, Piccioni F, Doench JG, Root DE, Hahn WC. ATXN1L, CIC, and ETS Transcription Factors Modulate Sensitivity to MAPK Pathway Inhibition. Cell Rep. 2017 Feb 7;18(6):1543-1557.
33. Kizhatil, K., Sandhu, N., Peachey, N. and Bennett, V., 2009. Ankyrin-B is required for coordinated expression of beta-2-spectrin, the Na/K-ATPase and the Na/Ca exchanger in the inner segment of rod photoreceptors. Experimental Eye Research, 88(1), pp.57-64.
34. Nag TC, Kathpalia P, Wadhwa S. Microtubule alterations may destabilize photoreceptor integrity: Age-related microtubule changes and pattern of expression of MAP-2, Tau and hyperphosphorylated Tau in aging human photoreceptor cells. Exp Eye Res. 2020 Sep;198:108153.
35. Grossman, G., Beight, C., Ebke, L., Pauer, G. and Hagstrom, S., 2014. Interaction of Tubby-Like Protein-1 (Tulp1) and Microtubule-Associated Protein (MAP) 1A and MAP1B in the Mouse Retina. Adv Exp Med Biol. 2014;801:511-8 pp.511-518.
36. Zhou, J. and Ekström, P., 2022. A Potential Role of Cyclic Dependent Kinase 1 (CDK1) in Late Stage of Retinal Degeneration. Cells, 11(14), p.2143.
37. Agca, C., Gubler, A., Traber, G., Beck, C., Imsand, C., Ail, D., Caprara, C. and Grimm, C., 2013. p38 MAPK signaling acts upstream of LIF-dependent neuroprotection during photoreceptor degeneration. Cell Death & Disease, 4(9), pp.e785-e785.
38. Zhang, J., Min, R., Le, K., Zhou, S., Aghajan, M., Than, T., Win, S. and Kaplowitz, N., 2017. The role of MAP2 kinases and p38 kinase in acute murine liver injury models. Cell Death & Disease, 8(6), pp.e2903-e2903.
39. Peyssonnaux, C. and Eychène, A., 2001. The Raf/MEK/ERK pathway: new concepts of activation. Biology of the Cell, 93(1-2), pp.53-62.
40. Dhillon AS, Meikle S, Yazici Z, Eulitz M, Kolch W. Regulation of Raf-1 activation and signalling by dephosphorylation. EMBO J. 2002 Jan 15;21(1-2):64-71.